Fluorescence of low-lying doubly photoexcited states in helium

M. Žitnik, K. Bučar, and M. Štuhec
J. Stefan Institute, Jamova 39, 1000 Ljubljana, Slovenia

F. Penent and R. I. Hall
DIAM, Université Pierre et Marie Curie, 75252 Paris Cedex 05, France

P. Lablanquie
LURE, Centre Universitaire Paris-Sud, Batiment 209D, Boîte Postale 34, 91898, Orsay, France
(Received 16 May 2001; published 1 March 2002)

In this work we investigate fluorescence decay of low-lying ($n \leqslant 8$) resonances with odd parity and total angular momentum $J=1$ below the $N=2$ threshold of helium. After discussing the photoabsorption cross section for creation of such states, we estimate the probability for the primary fluorescence transition to $1snl$ states below the first ionization threshold. The subsequent fluorescence cascade decay brings helium into the ground state or into one of the two long lived $1s2s\ ^{1,3}S$ states. We discuss the time scale of the cascade and combine all the calculated transition probabilities to determine branching ratios for singlet and triplet metastable production. Finally, we estimate the angular distribution of the emitted uv photons and perform a comparison with the recent experimental data of Penent *et al.* [Phys. Rev. Lett. **86**, 2758 (2001)].

DOI: 10.1103/PhysRevA.65.032520 PACS number(s): 32.70.Cs, 32.80.Dz

I. INTRODUCTION

Since the first observation of helium doubly excited states in photoabsorption spectra [1] it has been clear that satisfactory explanation of the measured data requires an explicit consideration of electron-electron correlations [2]. In the following years substantial progress was made both theoretically and experimentally; the experimental spectra were better resolved [3,4] following the improvement of synchrotron light sources, and original theoretical models were developed both to introduce different quantum numbers for simpler classification and understanding of these highly correlated states [5,6] and to precisely calculate their excitation and decay probabilities ([7] and references therein).

Autoionization to the He^+ continuum was considered from the beginning to be the strongest decay channel of doubly excited states and the ion yield measurements were taken as a fair measure of the absorption spectra. The fluorescence decay probability was believed to be negligible until the recent experimental search for metastable atoms and photons clearly showed the presence of fluorescence in the resonant decay scheme below the $N=2$ threshold [8]. It is easy to understand that the fluorescence transition of an inner electron should be more probable than autoionization, at least for high n, when the average interelectron separation becomes large. The limiting value of n depends on the character of the Rydberg series and may not be extremely high. In fact, for the $2pnd\ ^1P$ series fluorescence decay is already more probable than autoionization for the first member of the series [9]. The experimental study of autoionizing resonances $2s2p^6np\ ^1P$ in neon has also reported a signal coming from the fluorescence decay and showed that it dominates the autoionization for $n>27$ [10].

Another consequence of the ever larger separation of the Rydberg electron from the core is that fine (hyperfine) structure interaction of the inner electron with the nucleus becomes stronger than Coulomb interaction with the outer electron. When n approaches the threshold the LS coupling scheme turns into the jK coupling scheme [11]. This change is reflected in the shape of the helium fluorescence spectrum and calls for relativistic description of the process in the region of high Rydberg states. Indeed, an excellent agreement of the calculated jK fluorescence probabilities with the measured fluorescence yield was demonstrated close to the $N=2$ threshold [12]. In argon the low-lying LS-forbidden states were already observed in absorption in 1969 [13], and, very recently, also in photoelectron spectra as a pair of mirroring resonances in $Ar^+\ 3p^{-1}_{1/2,3/2}$ cross sections [14]. One of the first absorption spectra in neon taken with synchrotron light was interpreted completely within the LS coupling scheme except for the presence of two Rydberg series converging to the $Ne^+\ 2p^43s(^2P)$ threshold [15]. However, it is more surprising that at least two series of triplet resonances were clearly observed in the recent high-resolution photoexcitation study of helium below the $N=2$ threshold, this time in the fluorescence decay channel [16]. As determined from these measurements, the quantum defects of both series match very well the quantum defects of the $nd(^3D)$ and $n^-(^3P)$ series estimated by old nonrelativistic calculations [17].

A relatively simple technique, which favors observation of triplet states by the efficient detection of metastable atoms in combination with high-flux and high-resolution synchrotron light, makes it possible to observe triplet-singlet mixing already in the perturbative regime. The goal of this work is to model such mixing for low n values and to study its effect in the excitation and decay channels of helium doubly excited states. It complements the work done close to the threshold [12] and extends very recent calculations dealing with the decay of low-lying singlet resonances [18]. In our approach the fine structure interaction is added to the nonrelativistic Hamiltonian which is diagonalized for $J=1$ odd parity reso-

nances. For each of these states we calculate the excitation rate from the He ground state, the autoionization decay rate to the He^+ $1s$ continuum, and the fluorescence decay rate to the He* $1snl$ singly excited states below the first ionization threshold. Then we study the secondary fluorescence cascade and determine for each resonance the branching ratio to end up in one of the four long lived final states: the singlet and the triplet metastable state, the ground state of the helium atom, and the ground state of the helium ion. Finally, we discuss the angular distribution of uv photons emitted in the decay and combine all the calculated results to simulate the experimental spectrum [16].

II. DOUBLY EXCITED STATES

There are seven odd Rydberg series $n^{\pm}(^{1,3}P)$ and $nd(^{1,3}P,^3D)$ with $J=1$ converging to $2s_{1/2}^{-1}$ and $2p_{1/2,3/2}^{-1}$ thresholds in helium. It is not our intention to study different classification schemes of doubly excited states here so we use a compact version of the traditional notation [2] pointing out the dominant LS symmetry of the series. If necessary, the notation can be identified by energy ordering of the different series members, as in [17], and then translated to other notation [6].

A straightforward way to obtain these correlated states together with their energies is to diagonalize the Hamiltonian in some suitably chosen finite single configuration basis set. In the so-called truncated diagonalization method the base states are composed from the orthogonal hydrogenlike helium orbitals ($Z=2$) [17,19]. In the final version of our calculation each of the doubly excited states is expanded in the basis of 1058 single configurations, 393 of them with ^1P symmetry, 393 with ^3P, and 272 with ^3D. Each $^{1,3}P$ block consists of 121 sp configurations ($2s2p-12s12p$), 110 pd configurations ($2p3d-12p12d$), 90 df configurations ($3d4f-12d12f$) and 72 fg configurations ($4f5g-12f12g$). The ^3D block is without the sp configurations but otherwise the same. The chosen basis set allows good representation of resonances up to $n=8$, as shown by the smooth energy dependence of the quantum defects.

Several codes that can handle diagonalization in the orthogonal basis set are available in the ATOMIC STRUCTURE PACKAGE (ATSP) [20] and were easily adapted to the dimension of our problem. First we diagonalized the nonrelativistic Hamiltonian

$$H_{nr}=\hat{T}_1+\hat{T}_2-\frac{2}{r_1}-\frac{2}{r_2}+\frac{1}{r_{12}}, \tag{1}$$

and obtained 44 usable eigenstates,

$$|i^{2S+1}L\rangle=\sum_a c_{ia}|\alpha_a^{2S+1}L\rangle, \tag{2}$$

of ^1P, ^3P, or ^3D symmetry. The sum above runs over all single configurations included in the given LS block.

Due to the larger basis set we obtained 11 more states with up to 4 meV lower eigenenergies than reported in [17]. However, the $2^+(^1P)$ state, for example, was measured to have about 113 meV lower energy than our calculated value [4]. There are several specialized calculations, giving the energy of this singlet state just a few meV above the experimental value [7]. On the other hand, our calculation correctly reproduces the energy ordering of the states and finds their energies only a few meV away from the corresponding experimental values already at $n=5$ (Table I). The main deficiency of the method is the absence of $1s\epsilon p\ ^{1,3}P$ configurations which would account for the interaction with the continuum channel.

The next step of calculations was to add the spin-orbit interaction [20,21]

$$V_{so}=\alpha^2\left(\frac{\vec{l}_1\cdot\vec{s}_1}{r_1^3}+\frac{\vec{l}_2\cdot\vec{s}_2}{r_2^3}\right) \tag{3}$$

to Eq. (1) and repeat the diagonalization. The presence of Eq. (3) in the Hamiltonian destroys the LS block structure and causes mixing of different multiplets in the representation of the additional eigenstates. The ith resonance state R_i is now given by

$$\sum_{a=1}^{393} c_{ia}^{1P}|\alpha_a\ ^1P_1\rangle+\sum_{a=1}^{393} c_{ia}^{3P}|\alpha_a\ ^3P_1\rangle+\sum_{a=1}^{272} c_{ia}^{3D}|\alpha_a\ ^3D_1\rangle. \tag{4}$$

The inclusion of V_{so} does not cause any energy rearrangement of the states as compared to Eq. (2); only the eigenenergies of the dominantly triplet eigenstates change by a fraction of a meV. Adding further two fine structure terms to H_{nr}, namely, the spin-other-orbit V_{soo} and spin-spin V_{ss} terms [20,21], did not result in any notable change of eigenenergies and also did not change the mixing coefficients in Eq. (4). The relativistic shift operator V_{rs} [20], which would complete the second order relativistic corrections to the Hamiltonian, commutes with L and S and was omitted from the calculation. The magnitude and trend of mixing due to V_{so} can be seen in Fig. 1, where the two closest neighboring resonances (4) with dominant $n^+(^1P)$ and $nd(^3D)$ symmetry are projected onto the nonrelativistic LS multiplets (2) for $n=5$ and 8. For the resonances studied here, these mixing coefficients are much smaller than one, suggesting that indeed the same problem can be studied by first-order perturbation theory with the V_{so} interaction as a perturbation [16].

III. PHOTOABSORPTION, PRIMARY FLUORESCENCE, AND AUTOIONIZATION

The immediate effect of the spin-orbit mixing is that the photoexcitation probability of the first-order triplet states (4) becomes different from zero. To calculate the total ion production cross section σ_{ia} and the total primary fluorescence cross section σ_{ir} mediated by the ith resonance, a simple two-step model is employed. We have

$$\sigma_{ia}=\sigma_i\frac{\Gamma_i^a}{\Gamma_i^a+\Gamma_i^r},\quad \sigma_{ir}=\sigma_i\frac{\Gamma_i^r}{\Gamma_i^a+\Gamma_i^r},$$

TABLE I. Total photoabsorption cross section σ_i, autoionization rate Γ_i^a, primary fluorescence rate Γ_i^r, and effective asymmetry parameter β_i of the primary fluorescence for $J=1$ helium doubly excited states with $n \leqslant 8$. P_c, P_0, P_1, and P_2 are the probabilities of populating the He^+ ground state, He ground state, He $1s2s(^3S)$ state, and He $1s2s(^1S)$ state, respectively, via the resonance. β_{is} is the effective asymmetry parameter of the secondary uv fluorescence. The conversion of energy from a.u. to eV was made in the same way as in [17]. In the parentheses is the exponent P which multiplies the number in front by 10^p to obtain the value in the selected units. In the square brackets is the relative difference of the velocity to the length form results.

i	Dominant symmetry	Energy (eV)	σ_i (barns) (%)	Γ_i^a (ns^{-1})	Γ_i^r (ns^{-1}) (%)	β_i	P_c (%)	P_0 (%)	P_1 (%)	P_2 (%)	β_{is}
2	$2^+(^1P)$	60.2701	2.68(+4) [−13.1]	4.99(+4)	6.85(+0)[2.6]	−0.96	1.00(+0)	1.80(−5)	1.28(−12)	1.19(−4)	−0.02
6	3^+	63.6862	4.24(+3) [−23.2]	1.01(+4)	7.23(+0)[0.2]	−0.81	9.99(−1)	7.11(−4)	1.21(−9)	3.87(−6)	−0.07
13	4^+	64.4776	1.71(+3) [−23.1]	4.26(+3)	7.43(+0) [0.4]	−0.79	9.98(−1)	1.73(−3)	2.90(−8)	1.61(−5)	−0.08
20	5^+	64.8210	8.57(+2) [−23.1]	2.18(+3)	7.55(+0) [0.4]	−0.78	9.97(−1)	3.41(−3)	2.72(−7)	4.30(−5)	-0.09
27	6^+	65.0025	4.91(+2) [−23.1]	1.26(+3)	7.64(+0) [0.1]	−0.78	9.96(−1)	5.94(−3)	1.58(−6)	8.52(−5)	−0.09
34	7^+	65.1101	3.07(+2) [−23.1]	7.94(+2)	7.70(+0) [-0.1]	−0.77	9.90(−1)	9.45(−3)	6.71(−6)	1.45(−4)	−0.09
41	8^+	65.1792	2.05(+2) [−23.2]	5.33(+2)	7.73(+0) [-0.6]	−0.78	9.86(−1)	1.41(−2)	2.25(−5)	2.25(−4)	−0.09
3	$3^-(^1P)$	62.7710	9.92(+1) [64.1]	1.85(+2)	4.64(+0) [14.0]	−0.92	9.76(−1)	1.10(−2)	1.25(−8)	1.34(−2)	−0.03
10	4^-	64.1416	8.62(+1) [−9.0]	1.17(+2)	7.22(+0) [7.8]	−0.51	9.42(−1)	5.63(−2)	1.92(−7)	1.88(−3)	−0.19
17	5^-	64.6609	4.38(+1) [−11.5]	5.66(+1)	7.64(+0) [4.9]	−0.50	8.81(−1)	1.16(−1)	1.70(−6)	2.42(−3)	−0.19
24	6^-	64.9139	2.46(+1) [−13.2]	3.18(+1)	7.91(+0) [3.3]	−0.49	8.01(−1)	1.96(−1)	9.42(−6)	3.38(−3)	−0.20
31	7^-	65.0560	1.52(+1) [−15.0]	1.96(+1)	8.32(+0) [2.5]	−0.48	7.09(−1)	2.86(−1)	3.74(−4)	4.59(−3)	−0.20
38	8^-	65.1438	1.01(+1) [−17.0]	1.29(+1)	7.93(+0) [2.1]	−0.46	6.19(−1)	3.75(−1)	1.16(−4)	5.82(−3)	−0.21
9	$3d(^1P)$	64.1248	9.86(+0) [−88.1]	1.82(−1)	4.44(+0) [12.2]	−0.26	3.94(−2)	9.18(−1)	7.44(−6)	4.27(−2)	−0.29
16	$4d$	64.6518	7.59(+0) [−96.9]	3.57(−1)	4.02(+0) [6.8]	−0.23	8.16(−2)	8.97(−1)	2.10(−5)	2.09(−2)	−0.30
23	$5d$	64.9087	4.54(+0) [−97.3]	1.66(−1)	3.75(+0) [4.1]	−0.23	4.24(−2)	9.41(−1)	6.50(−5)	1.68(−2)	−0.30
30	$6d$	65.0528	2.61(+0) [−95.6]	4.56(−2)	3.51(+0) [3.2]	−0.23	1.28(−2)	9.71(−1)	1.80(−4)	1.56(−2)	−0.30
37	$7d$	65.1416	1.48(+0) [−91.2]	1.14(−2)	3.28(+0) [2.5]	−0.23	3.46(−3)	9.81(−1)	4.27(−4)	1.51(−2)	−0.30
44	$8d$	65.2006	1.11(+0) [−92.5]	1.54(−2)	3.02(+0) [2.2]	−0.16	5.07(−3)	9.80(−1)	8.70(−4)	1.42(−2)	−0.32
1	$2^+(^3P)$	58.3683	6.72(−4) [−13.1]	3.09(+4)	5.82(+0) [18.9]	0.50	1.00(+0)	5.58(−13)	1.88(−4)	4.14(−12)	−0.01
4	3^+	63.1295	9.19(−4) [−9.2]	9.00(+3)	4.96(+0) [10.7]	0.47	9.99(−1)	6.73(−11)	5.51(−4)	2.43(−11)	−0.15
11	4^+	64.2502	2.55(−3) [−10.5]	3.47(+3)	4.83(+0) [6.1]	0.45	9.99(−1)	1.73(−9)	1.39(−3)	1.37(−10)	−0.19
18	5^+	64.7082	5.69(−3) [−10.8]	1.57(+3)	4.82(+0) [3.9]	0.44	9.97(−1)	2.03(−8)	3.06(−3)	8.27(−10)	−0.19
25	6^+	64.9386	1.07(−2) [−11.0]	8.75(+2)	4.82(+0) [2.4]	0.44	9.95(−1)	1.34(−7)	5.47(−3)	3.75(−9)	−0.17
32	7^+	65.0705	1.82(−2) [−11.1]	5.33(+2)	4.75(+0) [2.1]	0.44	9.91(−1)	6.28(−7)	8.84(−3)	1.43(−8)	−0.16
39	8^+	65.1530	2.86(−2) [−11.3]	3.48(+2)	4.59(+0) [1.1]	0.44	9.87(−1)	2.26(−6)	1.30(−2)	4.66(−8)	−0.15
5	$3^-(^3P)$	63.2617	7.49(−4) [−17.6]	3.12(+1)	7.39(+0) [0.1]	0.36	8.08(−1)	2.86(−9)	1.92(−1)	1.05(−8)	−0.03
12	4^-	64.3293	2.76(−3) [−20.2]	8.95(+0)	7.88(+0) [0.3]	0.33	5.32(−1)	3.71(−7)	4.68(−1)	2.32(−8)	−0.18
19	5^-	64.7512	6.44(−3) [−20.9]	4.18(+0)	8.03(+0) [0.1]	0.32	3.42(−1)	2.91(−6)	6.57(−1)	8.20(−8)	−0.21
26	6^-	64.9639	1.22(−2) [−21.3]	2.34(+0)	8.08(+0) [0.1]	0.32	2.25(−1)	1.27(−5)	7.75(−1)	2.60(−7)	−0.21
33	7^-	65.0864	2.07(−2) [−21.5]	1.46(+0)	8.04(+0) [0.3]	0.32	1.54(−1)	3.99(−5)	8.46(−1)	7.13(−7)	−0.22
40	8^-	65.1636	3.22(−2) [−21.7]	1.01(+0)	7.68(+0) [0.0]	0.32	1.14(−1)	1.00(−4)	8.86(−1)	1.68(−6)	−0.22
7	$3d(^3D)$	63.7936	5.33(−3) [−27.9]	1.17(−2)	9.88(+0) [0.0]	0.13	1.18(−3)	8.05(−7)	9.99(−1)	2.45(−9)	−0.02
14	$4d$	64.5146	2.22(−2) [−27.3]	5.12(−2)	9.96(+0) [0.0]	0.13	5.11(−3)	7.58(−7)	9.95(−1)	7.42(−8)	−0.02
21	$5d$	64.8385	5.42(−2) [−27.1]	1.28(−1)	9.98(+0) [0.0]	0.13	1.27(−2)	3.67(−5)	9.87(−1)	4.96(−7)	−0.02
28	$6d$	65.0122	1.05(−1) [−27.0]	2.50(−1)	9.99(+0) [0.0]	0.13	2.44(−2)	1.24(−4)	9.75(−1)	1.90(−6)	−0.03
35	$7d$	65.1160	1.78(−1) [−27.0]	4.27(−1)	9.98(+0) [0.0]	0.13	4.10(−2)	3.36(−4)	9.59(−1)	5.46(−6)	−0.03
42	$8d$	65.1831	2.77(−1) [−27.0]	6.66(−1)	9.92(+0) [0.0]	0.13	6.29(−2)	7.60(−4)	9.36(−1)	1.29(−5)	−0.03
8	$3d(^3P)$	64.0775	1.26(−3) [−57.6]	1.88(+1)	6.58(+0) [12.3]	0.09	7.41(−1)	1.03(−6)	2.59(−1)	2.23(−8)	−0.32
15	$4d$	64.6243	3.28(−3) [−50.5]	9.92(+0)	6.52(+0) [7.1]	0.10	6.03(−1)	3.48(−6)	3.97(−1)	5.04(−8)	−0.30
22	$5d$	64.8927	6.73(−3) [−48.1]	5.57(+0)	6.51(+0) [4.7]	0.11	4.61(−1)	1.21(−5)	5.39(−1)	1.62(−7)	−0.29
29	$6d$	65.0430	1.18(−2) [−47.0]	3.24(+0)	6.53(+0) [2.7]	0.11	3.32(−1)	3.60(−5)	6.68(−1)	4.80(−7)	−0.28
36	$7d$	65.1353	1.88(−2) [−46.7]	1.94(+0)	6.42(+0) [2.7]	0.11	2.32(−1)	9.13(−5)	7.68(−1)	1.24(−6)	−0.28
43	$8d$	65.1961	2.69(−2) [−46.4]	1.25(+0)	6.12(+0) [1.9]	0.10	1.69(−1)	1.71(−4)	8.30(−1)	2.35(−6)	−0.28

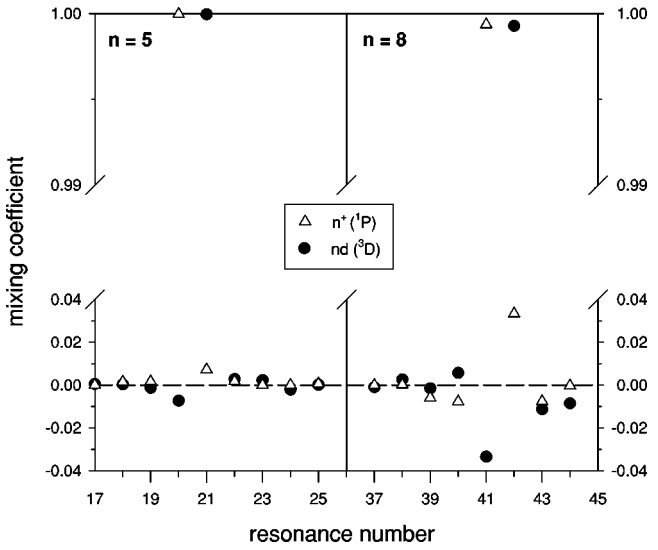

FIG. 1. A pair of neighboring resonances (4) with dominant $n^+(^1P)$ and $nd(^3D)$ symmetry projected on the basis of pure LS multiplets (2) for $n=5$ and $n=8$.

where σ_i is the photoabsorption cross section integrated over the incoming photon energies, and Γ_i^a, Γ_i^r are the autoionization and fluorescence decay rates of the ith resonance, respectively. This model, often applied to the reverse process of dielectronic recombination [22], was chosen recently to discuss the observed fluorescence intensity emitted in decay of Rydberg states as a function of the effective quantum number in helium and neon [9,10]. The same approach with completely uncoupled photoabsorption, photoemission, and autoionization is used here to study quantitatively the fluorescence of the lowest-lying doubly excited states in helium.

The expansion coefficients c_{jb} and eigenenergies E_j of the ground state and of the singly excited even states $1sns\,^{1,3}S$ and $1snd\,^{1,3}D$ of helium, populated via primary fluorescence,

$$|j^{2S+1}L'\rangle = \sum_b c_{jb} |\alpha_{jb}\,^{2S+1}L'\rangle, \tag{5}$$

were calculated one by one up to $n=8$ within the multiconfigurational Hartree-Fock (MCHF) approximation [20].

The energy integrated photoabsorption cross section for helium to pass from the ground state to the doubly excited state R_i with energy E_i, proportional to the corresponding oscillator strength, is given by [11]

$$\sigma_i = \frac{4}{3}\pi^2 \alpha E_{i0} S_{i0}(^1S \rightarrow {}^1P), \tag{6}$$

where $E_{i0}=E_i-E_0$ and

$$S_{i0}(^1S \rightarrow {}^1P) = \left| \sum_{a,b} c_{ia}^{1P} c_{0b} \langle \alpha_{ia}\,^1P || \mathbf{E}^1 || \alpha_{0b}\,^1S \rangle \right|^2 \tag{7}$$

is the line strength in the length form. E_q^1 is the qth component of the atomic electric dipole tensor operator,

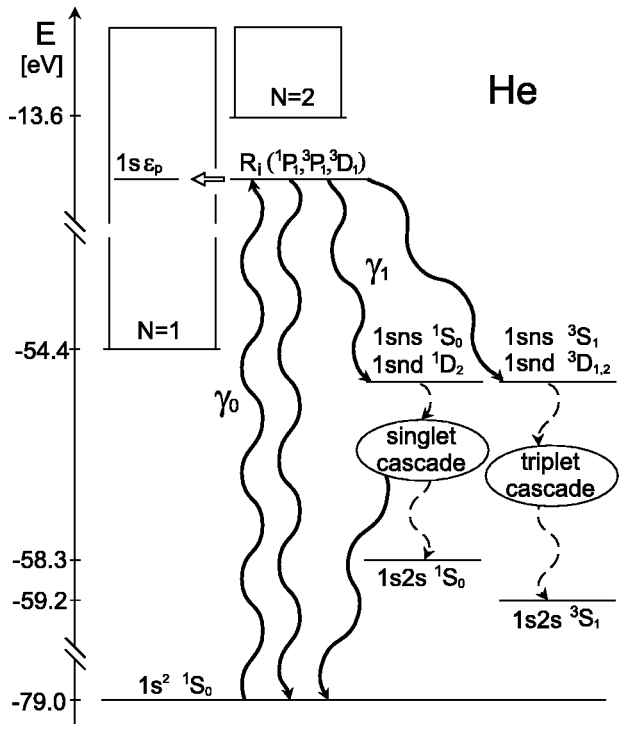

FIG. 2. Schematic decay scheme of the resonance R_i. uv photons are denoted by full lines.

$$\sqrt{\frac{4\pi}{3}}[r_1 Y_q^1(\hat{1}) + r_2 Y_q^1(\hat{2})].$$

Note that only the transition amplitude to the ^1P expansion block of the resonance differs from zero in this approximation. The line strengths in length and velocity form were calculated by the ATSP codes, which can handle multipole transitions between the nonorthogonal LS-coupled states [20].

Once the resonance is created it may release energy by the fluorescence transition into one of the four series of states converging to the first ionization threshold (Fig. 2). Due to the dipole selection rules only the following block transitions populate the singly excited states (5):

$$^1P_1 \rightarrow 1sns(^1S_0), 1snd(^1D_2),$$

$$^3P_1 \rightarrow 1sns(^3S_1), 1snd(^3D_{1,2}),$$

$$^3D_1 \rightarrow 1snd(^3D_{1,2}). \tag{8}$$

The partial fluorescence rate Γ_{ji}^r of the ith resonance ending in the jth state (5) is obtained by multiplying $(4/3)\alpha^3(E_i - E_j)^3$ by

$$\frac{1}{3}S_{ji}(^1P \rightarrow {}^1S), \quad \frac{1}{3}S_{ji}(^1P \rightarrow {}^1D), \quad \frac{1}{3}S_{ji}(^3P \rightarrow {}^3S),$$

$$\frac{1}{3}S_{ji}(^3P \rightarrow {}^3D) + \frac{1}{5}S_{ji}(^3D \rightarrow {}^3D) \tag{9}$$

for $1sns(^1S)$, $1snd(^1D)$, $1sns(^3S)$, and $1snd(^3D)$ final states, respectively. The line strengths above are defined by

$$S_{ji}(^{2S+1}L \rightarrow {}^{2S+1}L') = \left| \sum_{b,a} c_{jb} c_{ia}^{(2S+1)L} \langle \alpha_{jb}\, {}^{2S+1}L' || \mathbf{E}^1 || \alpha_{ia}\, {}^{2S+1}L \rangle \right|^2, \tag{10}$$

similar to Eq. (7). The partial fluorescence rates are presented in Fig. 3 for the seven $J=1$ resonances with $n=5$. The total primary fluorescence rates

$$\Gamma_i^r = \sum_j \Gamma_{ji}^r \tag{11}$$

for all the resonances with $n \leqslant 8$ are reported in Table I.

Exactly the same representation of the resonant states was employed to calculate the autoionization decay rates

$$\Gamma_i^a = 2\pi [|A_i(^1P)|^2 + |A_i(^3P)|^2], \tag{12}$$

where

$$A_i(^{1,3}P) = \sum_a c_{ia}^{1,3P} \langle 1s\epsilon p\, {}^{1,3}P | r_{12}^{-1} | \alpha_{ia}\, {}^{1,3}P \rangle.$$

The continuum wave was approximated by a $Z=1$ Coulomb wave after checking that a negligibly small phase difference is acquired by the wave due to incomplete screening of the nuclear charge by the $1s$ electron. The wave was calculated for five different energies between 34 eV and 40 eV to be well represented in the energy region of the resonant states. Note that only the *p*-wave amplitude contributes to the decay rate due to the scalar nature of the Coulomb operator. According to the selection rules the autoionization from the ^3D expansion block of the resonance may give final states only above the $N=2$ threshold in helium, which, however, are not accessible by energy conservation.

IV. SECONDARY FLUORESCENCE

The singly excited states created by primary fluorescence may further decay relatively fast by secondary photon emission ending up in any of the allowed singly excited states of lower energy,

$$1sns(^{1,3}S) \rightarrow 1smp(^{1,3}P),$$

$$1snd(^{1,3}D) \rightarrow 1smp(^{1,3}P), 1smf(^{1,3}F). \tag{13}$$

These newly populated states may again release their energy by fluorescence. The series of decays definitely stops when helium arrives at the ground state. However, due to the relatively long lifetimes of 10^4 s and 20 ms [23,24], the lowest two excited states $1s2s\,{}^3S$ and $1s2s\,{}^1S$ can be taken as metastable, at least on the time scale of recent experiments detecting decay products of doubly excited states.

In order to follow the cascade we have calculated the dipole transition rates for all pairs of $1snl$ states with $n \leqslant 8, l \leqslant 3$. For this purpose we have calculated odd singly excited states (13) populated in the first step of the cascade, again by the MCHF procedure. The comparison of our *ab initio* calculation to the previously published fluorescence rates has shown that agreement is better than 1% [25].

The calculated rates were fed as parameters into the system of coupled differential equations that govern the time evolution of the level populations in the selected set. In addition to the resonance, the set contained even and odd singly excited states (singlets and triplets), together with the ground state, and the continuum $1s\epsilon p$. If all calculated singly excited states are ordered by increasing energy and counted by index *k*, the equations are

$$\dot{P}_i = -\left(\Gamma_i^a + \sum_{k=j} \Gamma_{ki}^r \right) P_i,$$

$$\dot{P}_c = \Gamma_i^a P_i,$$

$$\dot{P}_k = \sum_{q>k} \Gamma_{kq}^r P_q - \left(\sum_{q<k} \Gamma_{qk}^r \right) P_k, \tag{14}$$

where, respectively, P_i, P_c, and P_k denote the population of the *i*th resonance, population of the continuum, and population of the *k*th singly excited state, including the ground ($k=0$), the triplet metastable ($k=1$) and the singlet metastable states ($k=2$). Finally, for each resonance the system was integrated starting from initial conditions $P_i=1$, $P_c=0$, and $P_k=0$ for all *k* in order to obtain the level populations at any subsequent time. At any time

$$P_i + P_c + \sum_k P_k = 1.$$

The integration was stopped after approximately 20 μs when the state populations other than P_c, P_0, P_1, and P_2 have dropped to less than 10^{-20}. Note that the continuum channel is not really coupled to the other levels; it is being filled only from the resonance. The singlet and triplet subsets of the singly excited state manifold were assumed to evolve independently, in the true nonrelativistic manner (Fig. 2). To verify the results, we have determined the converged populations P_c, P_0, P_1, and P_2 independently by a Monte Carlo simulation, generating a large number of photon cascades starting from the resonance R_i to end up in any of the four long lived end states. At each step of the cascade the final state was chosen randomly among the allowed states, in proportion to the fluorescence rates connecting the given initial to the allowed final states.

The special interest of this work is to determine the populations of both metastable states and the ground state several microseconds after the creation of the doubly excited state. This is closely related to the quantitative interpretation of the recent experimental results [16].

V. ANGULAR DISTRIBUTION

The change of the atomic linear momentum due to absorption and emission of uv photons is negligible. Virtually

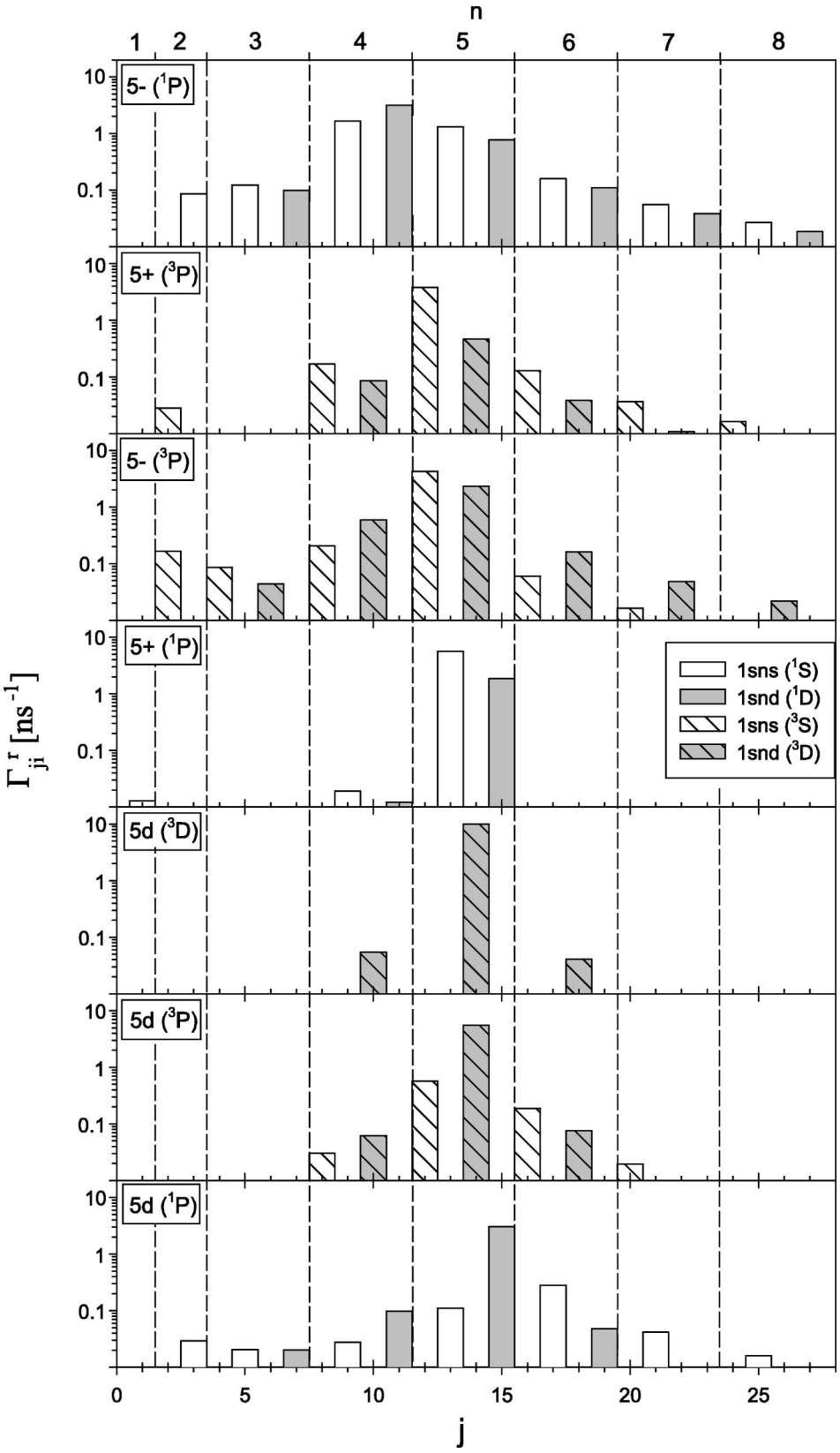

FIG. 3. The partial fluorescence rates of $n=5$ resonances to decay into $1snsns$ and $1snd$ singlet and triplet states. The final states are counted by j in order of increasing energy.

all the metastable atoms created by relaxation of doubly excited states will hit a detector surface placed perpendicularly and centered on the line that connects the gas nozzle to the pointlike target volume. On the other hand, the photons are emitted into the whole solid angle and, in general, the measured signal will depend on the angular position of the detector. In order to study the angular distribution of the primary fluorescence

$$1s^2(^1S_0)+\gamma_0 \rightarrow R_i \rightarrow 1s(ns,nd)+\gamma_1, \qquad (15)$$

we start from the well-known general form of the photoabsorption-photoemission cross section [26], differential in angle of the emitted photon γ_1,

$$\frac{d\sigma_{ji}^r}{d\Omega_1}=\frac{\sigma_{ji}^r}{4\pi}[1+\beta_{ji}P_2(\hat{k}_1\cdot\hat{\epsilon}_0)]. \tag{16}$$

Here $\hat{\epsilon}_0$ denotes the polarization of the incoming light and $\hat{k}_1$ the direction of the emitted photon. The total cross section for reaction (15) is again approximated by

$$\sigma_{ji}^r=\sigma_i\frac{\Gamma_{ji}^r}{\Gamma_i^a+\Gamma_i^r},$$

where all the quantities above were previously defined by Eqs. (6), (9), (11), and (12). To determine the asymmetry parameter β_{ji} we explicitly express the differential cross section (16),

$$\frac{d\sigma_{ji}^r}{d\Omega_1}\propto\frac{1}{2J_0+1}\sum_{M_0M_j\nu}\left|\sum_{M_i}\langle\alpha_jJ_jM_j|\hat{\epsilon}_1^{\nu}\cdot(\mathbf{r}_1+\mathbf{r}_2)|\alpha_iJ_iM_i\rangle\right.$$
$$\left.\times\langle\alpha_iJ_iM_i|\hat{\epsilon}_0\cdot(\mathbf{r}_1+\mathbf{r}_2)|\alpha_0J_0M_0\rangle\right|^2, \tag{17}$$

as proportional to the absolute square of the product of the photoabsorption and photoemission amplitudes, averaged over the initial and summed over the final projections of the total angular momentum and over the two perpendicular polarizations ν of the emitted photon [27].

The initial state is represented by the quantum numbers $\alpha_0J_0M_0$, the intermediate state by $\alpha_iJ_iM_i$, and the final atomic state after fluorescence by $\alpha_jJ_jM_j$. The expression on the right side of Eq. (17) can be simplified to assume a form proportional to Eq. (16). Then it is easy to extract the asymmetry parameter, which is given by

$$\beta(J_0,J_i,J_j)=-\frac{\begin{Bmatrix}J_i & 2 & J_i\\ 1 & J_0 & 1\end{Bmatrix}\begin{Bmatrix}J_i & 2 & J_i\\ 1 & J_j & 1\end{Bmatrix}}{\begin{Bmatrix}J_i & 0 & J_i\\ 1 & J_0 & 1\end{Bmatrix}\begin{Bmatrix}J_i & 0 & J_i\\ 1 & J_j & 1\end{Bmatrix}}, \tag{18}$$

in accordance with [26]. Via 6-j symbols, the parameter depends only on the total angular momenta of the atomic states involved and not on any other quantum numbers that describe these states. In our case $J_0=0$, $J_i=1$, but J_j can be 0, 1, or 2. The asymmetry parameters for the three values of the final angular momentum are

$$\beta_0=-1,\quad \beta_1=\frac{1}{2},\quad \beta_2=-\frac{1}{10}. \tag{19}$$

The angular distribution of photons emitted from the R_i resonance depends on the relative contributions of different J_j values in the composition of the final singly excited state. Since the $1sns(^1S)$, $1snd(^1D)$, and $1sns(^3S)$ final states are characterized by a unique value of J_j, the corresponding asymmetry parameters β_{ji} are simply given by β_0, β_2, and β_1. If j denotes one of the $1snd(^3D)$ final states then the expression for β_{ji} becomes slightly more complicated due to the interference of fluorescence amplitudes originating from the ^3P and ^3D expansion blocks of the resonance. These two blocks both populate $1snd(^3D)$ final states with either one or two times the total angular momentum. In the case considered here the resonances have one major symmetry and the interference can be neglected. The asymmetry parameter is then approximately equal to

$$\frac{1}{4}\beta_1+\frac{3}{4}\beta_2=\frac{1}{20},\quad \frac{3}{4}\beta_1+\frac{1}{4}\beta_2=\frac{63}{500} \tag{20}$$

for the major ^3P and ^3D symmetries of the resonance, respectively.

Finally, to determine the effective angular distribution of the primary fluorescence originating from the ith resonance, β_{ji} has to be averaged over the partial fluorescence decay rates leading to various final singly excited states j, that is,

$$\beta_i=\frac{1}{\Gamma_i^r}\sum_j\Gamma_{ji}^r\beta_{ji}.$$

The effective asymmetry parameters β_i are presented in Table I.

Our goal is to compare our calculations with the measurements performed with a simple microchannel plate (MCP) detector [16]. It is necessary then to estimate the angular distribution of all uv photons emitted in the fluorescence decay channel of doubly excited states. In addition to that of the primary fluorescence we need to know the angular distribution of the secondary photons emitted during the subsequent cascade decay. Actually, we are interested only in photons emitted in the last step of the cascade, which brings the atom into the ground state. Only these photons have high enough energy to be detected by the simple detector. To a good approximation, there are no secondary uv photons emitted in the cascade decay of triplet singly excited states. On the other hand, a large majority of singlet states created by the primary fluorescence end in the ground state. The total yield of secondary uv photons is then expected to be comparable to the primary photon yield and has to be accounted for properly.

There are two by far the most probable types of singlet cascade that end by emission of the secondary uv photon γ_3,

$$\begin{array}{ccccc} & & 1sns[0]+\gamma_1 & & \\ & \nearrow & & \searrow & \\ & & A & & \\ \gamma_0\rightarrow R_i[1] & & & & 1smp[1]+{}_2\rightarrow 1s^2[0]+\gamma_3. \\ & \searrow & & \nearrow & \\ & & B & & \\ & & 1snd[2]+\gamma_1 & & \end{array} \tag{21}$$

Here $m<n$ because of energy conservation. Each type of cascade is specified by a unique pattern of the total angular momenta $[J]$ of atomic states through which it proceeds. The

angular distribution of the emitted photons depends on this pattern only and not on the other quantum numbers. For the *A* type of cascade it is immediately clear that emission of γ_2 and γ_3 should be isotropic, because their ''parent'' state $1sns(^1S_0)$ has no preferred direction in space, so $\beta_A=0$. The angular distributions of γ_2 and γ_3 in case *B* may be obtained by the straightforward extension of method (17). The amplitude of the cascade (21) is given by a product of four single-step amplitudes, summed over angular momentum projections of the three intermediate states. After writing each single-step operator in tensorial form, applying the Wigner-Eckart theorem, and summing the absolute squares over two perpendicular polarizations of each of the three emitted photons, the angular part of the differential cross section is extracted:

$$\sum_{\nu,\tau,\rho=1}^{2}\left|\sum_{M_1M_2}\begin{pmatrix}1 & 1 & 2\\ -M_2 & M_2-M_1 & M_1\end{pmatrix}\begin{pmatrix}2 & 1 & 1\\ -M_1 & M_1 & 0\end{pmatrix}\times Y_1^{M_1^*}(\hat{\epsilon}_1^{\nu})Y_1^{M_1-M_2}(\hat{\epsilon}_2^{\tau})Y_1^{M_1}(\hat{\epsilon}_3^{\rho})\right|^2.$$

To determine the angular distribution of each photon separately the cross section has to be integrated over the angles of the remaining two photons. In case *B* the asymmetry parameter turns out to be the same for γ_2 and γ_3 photons,

$$\beta_B=-\frac{7}{20}.$$

The effective angular distribution of γ_3 for each resonance is obtained by averaging the two asymmetry parameters β_A and β_B, weighted by the probability to decay via path *A* or *B*, respectively. The effective asymmetry parameter β_{is} of the secondary uv photon is then

$$\beta_{is}=\beta_B\frac{\sum_{j'}\Gamma^r_{j'i}}{\sum_j\Gamma^r_{ji}}.$$

The summation in the numerator goes over $1snd(^1D)$ states only and in the denominator over $1snd(^1D)$ and $1sns(^1S)$ states (Table I).

VI. RESULTS AND COMMENTS

There is a large number of papers dealing with autoionization of helium doubly excited singlet states [7]. Apart from the large relative difference among the total photoabsorption cross sections of different singlet series, it is well known that within the series the cross sections varies as the inverse of the third power of the effective quantum number $n_s=n-\delta_s$, roughly following the *n* dependence of the square of the Rydberg orbital amplitude in the core region [9,10]. Much less theoretical work has been published on the fluorescence decay of these doubly excited states [18,28] and, to our knowledge, no calculations are available that consider photoexcitation and decay of the triplet resonances. Based on this work there is a short discussion of the total photoabsorption cross section of the triplet resonances in [16], which explains the observed n_s^3 rise by the presence of spin-orbit perturbation.

By inspecting the results in Table I we find, as in the singlet case, one strongly autoionizing triplet series, denoted by $n^+(^3P)$, for which the autoionization rate reaches about 60% of the $n^+(^1P)$ rate. Then there are two triplet series with comparable autoionization rates, namely, $n^-(^3P)$, reaching 30%, and $nd(^3P)$, reaching about 10% of the $n^-(^1P)$ autoionization decay rate, respectively. The fourth triplet series, $nd(^3D)$, autoionizes about ten times slower than the weakest singlet series $nd(^1P)$ at $n=3$. However, the autoionization rate increases for higher Rydberg states and at $n=8$ the decay becomes more than ten times faster than the decay of $nd(^1P)$, due to the 0.16% of singlet $n^+(^1P)$ admixture (Fig. 1).

On the other hand, the most strongly excited triplet series $nd(^3D)$ displays the largest fluorescence decay rate of all seven series (Table I). Reaching about 10 ns^{-1}, the rate is essentially equal to that of the $2p\rightarrow1s$ transition in the helium ion. Previous modeling assumed that the fluorescence rate of every singlet series converges fast to this limiting value [9]. But such behavior seems to be more the exception than the rule. We found, as in [18], that the fluorescence rate of the doubly excited state, even with $n=8$, can be considerably smaller than the fluorescence rate of $2p$ electrons in the helium ion, due to the correlated motion of the two electrons. We can understand this qualitatively as a kind of polarization effect in the body frame where the outer electron forces the inner electron into some series specific mixture of $2s$ and $2p$ orbitals. The larger is the weight of the $2s$ orbital in this combination, the smaller is the probability of the inner electron fluorescing into the $1s$ orbital. Due to this effect the $nd(^1P)$ series appears to have the smallest primary fluorescence rate, roughly equal to 3.0 ns^{-1}. The second weakest is the $n^+(^3P)$ series, still having a fluorescence rate less than one-half of the upper limiting value of 10 ns^{-1}, at $n=8$. The next is the $nd(^3P)$ series with Γ_i^r of about 6 ns^{-1}. Finally, the three series $n^+(^1P)$, $n^-(^1P)$, and $n^-(^3P)$ have nearly equal total fluorescence rates of about 8 ns^{-1}. We note that our calculated linewidth of the $nd(^1P)$ resonance is 3.04 μeV, which agrees reasonably well with 3.3 μeV, the lower limit as determined recently by [29].

Figure 3 presents primary fluorescence rates for $n=5$ resonances. The decay rate distribution of higher-lying resonances follows a similar pattern shifted in parallel according to the *n* value of the resonance. The distribution of the total decay rate among $1sns$ and $1snd$ final states reflects the composition of the initial correlated state. For example, the $5d(^3D)$ resonance fluoresces almost fully into $1s5d(^3D)$ and its oscillator strength matches almost perfectly the oscillator strength of the $2p\rightarrow1s$ transition in the helium ion. All this points to a very simple structure of the resonance state, and, in fact, the Hartree-Fock energy of a single $2p5d(^3D)$ configuration is just about 3 meV higher than the energy of the corresponding correlated state. The most correlated series

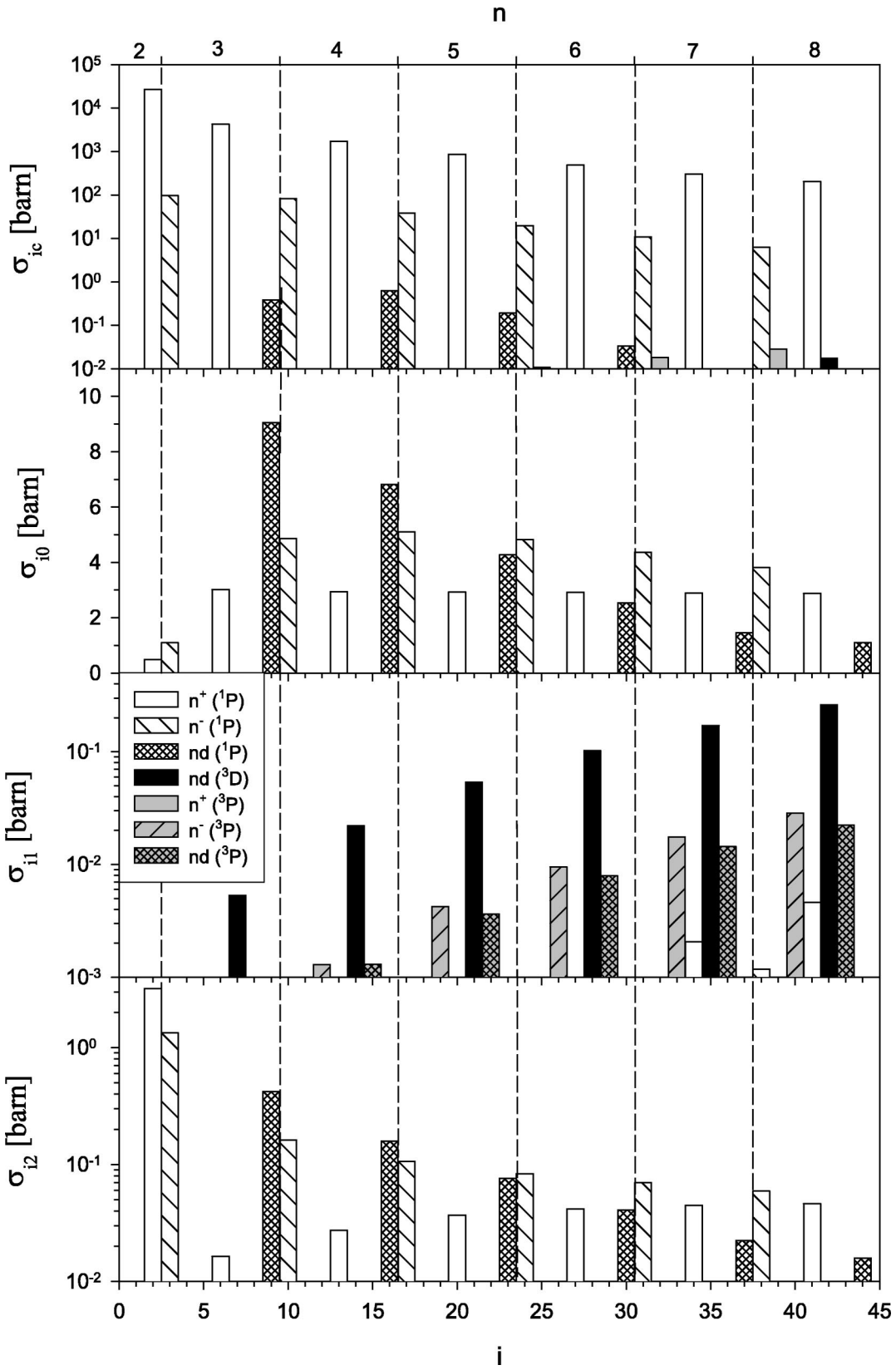

FIG. 4. The calculated cross section for populating the ground state of the ion (σ_{ic}), the ground state of the atom (σ_{i0}), the triplet metastable state (σ_{i1}), and the singlet metastable state (σ_{i2}) via decay of the ith resonance.

in the sense of requiring the largest MCHF expansion is $n^-(^{1,3}P)$, for which the ratio of oscillator strengths into $1snsn$ and $1snd$ states is close to 1 (Fig. 4). For the $n^+(^1P)$ and $n^+(^3P)$ series the ratio is close to 3 and 8, respectively, in favor of $1snsn$ final states. Finally, for $nd(^{1,3}P)$ series the ratio is about 10 in favor of $1snd$ final states. We note that the primary fluorescence most likely occurs in the frozen Rydberg electron mode, that is, from a given n resonance state into the $1snsn$ or $1snd$ final state with the same n. The strong exceptions to the rule are $n^-(^1P)$ resonances, having relatively large oscillator strength into $1s(n-1)(s,d)$ states. Such a delayed onset nearly doubles the total fluorescence decay rate of this series at $n=4$ as compared to $n=3$. A slight decrease of the total fluorescence rates at high n (Table I) is due to decays into the $1s(n\geqslant 9)l$ final states, not accounted for by our calculation. The creation of the triplet (singlet) singly excited states in decay of the predominantly singlet (triplet) resonance is too weak to be seen in Fig. 4. The strongest ''forbidden'' primary fluorescence transitions within the range of our calculations are $8^+(^1P) \rightarrow 1s8d(^3D)$ and $8d(^3D)\rightarrow 1s8s(^1S)$ with decay rates of 0.011 ns^{-1} and 0.0074 ns^{-1}, respectively.

In Table I we present for each resonance the probability of ending up in the ground state of He^+, in the atomic ground state, in the triplet $1s2s$ metastable state, and in the singlet $1s2s$ metastable state. In previous work the ratio of the singlet metastable to the ground state population was estimated to be about 3% [8]. This comes from the assumption that all low-lying $1smp$ states which are mainly populated in the second step of the cascade (21) have branching ratio of 3%. However, the most likely populated state is $1s2p$, having a branching ratio of only 0.1%. The true branching ratio P_2/P_0 is thus actually lower, approaching 1.5% for $n=8$. Except for the $3d(^3D)$ resonance the ratio is largest for the lowest members of the resonance series, reaching values even larger than 1 for $3^\pm(^{1,3}P)$, due to strong formation of $1s2s(^1S)$ directly from the resonance state. The population ratio of the triplet metastable to the ground state, P_1/P_0, decreases with increasing n for the triplet dominated resonances, but is still more than 1000 at $n=8$. Due to the singlet-triplet mixing, more and more oscillator strength goes into the singlet manifold of states, which predominantly populates the ground state. The opposite is true for the singlet dominated resonances. Due to the mixing, the triplet metastable state is more and more populated, causing the increase of P_1/P_0 with n.

The ratio of the ion state population to the ground state population, P_c/P_0, reflects the behavior of Γ_i^a except for the $nd(^3D)$ series. While the autoionization rate increases with n, fewer and fewer ions are produced compared to the atoms in the ground state, despite a nearly constant fluorescence rate. The same triplet-singlet mixing responsible for the increase of Γ_i^a distributes oscillator strength to the singlet manifold of states, causing more and more $nd(^3D)$ resonances to decay into the ground state. Combining the two, the second effect prevails due to the relatively large Γ_i^r.

The cross section for production of the four long lived final states via the resonance R_i is obtained by multiplying the total photoabsorption cross section by the corresponding converged population (Fig. 4),

$$\sigma_{i0}=\sigma_i P_0, \quad \sigma_{i1}=\sigma_i P_1, \quad \sigma_{i2}=\sigma_i P_2, \quad \sigma_{ic}=\sigma_i P_c.$$

The ground state production cross section σ_{i0} shows various trends ranging from n_s^{-3} for the $nd(^1P)$ series to nearly a constant for the $n^+(^1P)$ series, which is consistent with the prediction of the simple Rydberg model [9,10]. σ_{i2} follows σ_{i0} scaled down to 1.5% as soon as the population ratio stabilizes (Table I). The largest cross sections σ_{i1} for the triplet metastable production, almost equal to the excitation cross section σ_i, is calculated for the $nd(^3D)$ series. The metastable production under the other triplet resonances rises even faster than n^3 but then slows down to follow the excitation cross section, as soon as $\Gamma_i^r \gg \Gamma_i^a$. It is interesting that triplet metastable production under the singlet $n^+(^1P)$ line is larger than under the triplet $n^+(^3P)$ line, a combined effect of much larger but decreasing excitation cross section and small but strongly increasing triplet admixture in the singlet state. According to our results, the largest ion yield of the triplet resonances is given by the $n^+(^3P)$ series. Due to its relatively isolated energy position between the $n^-(^1P)$ and $n^+(^1P)$ resonances, this is the best candidate to be detected in future experiments in the ion detection channel. Still, the ion yield due to the $8^+(^3P)$ resonance is expected to be about 100 times smaller than the yield under the $8^-(^1P)$ resonance.

The effective asymmetry parameter β_i turns out to be negative for the singlet dominated resonances and positive for the triplet dominated resonances, a consequence of the preferred final states (Table I). The primary fluorescence from the singlet $n^+(^1P)$ states is expected to have the largest anisotropy; these resonances preferably decay into $1snsn$ states for which $\beta_{ji}=-1$. The primary photon emission from $nd(^3P)$ resonances is almost isotropic, $\beta_i=0.10$. As shown by our calculation, the secondary uv photons are emitted slightly asymmetrically with respect to the polarization direction; the effective asymmetry parameter for such transitions is in the range $-7/20<\beta_{is}<0$, where the upper and the lower limits are imposed by decay paths A and B [Eq. (21)], respectively. By measuring the asymmetry parameters of uv photons we might gain more insight into the resonance decay dynamics and structure of the states involved.

VII. COMPARISON TO THE EXPERIMENTAL DATA

Below we compare our results to the recent data [16] recorded at the high-resolution high-flux gas phase photoemission beamline at the synchrotron Elettra [30]. The differential cross section for emission of uv photons in decay of the ith resonance is

$$\frac{d\sigma_i^{uv}}{d\Omega}=\frac{\sigma_{i0}+\sigma_{i1}+\sigma_{i2}}{4\pi}[1+\beta_i P_2(\cos\theta)] + \frac{\sigma_{i0}}{4\pi}[1+\beta_{is}P_2(\cos\theta)], \tag{22}$$

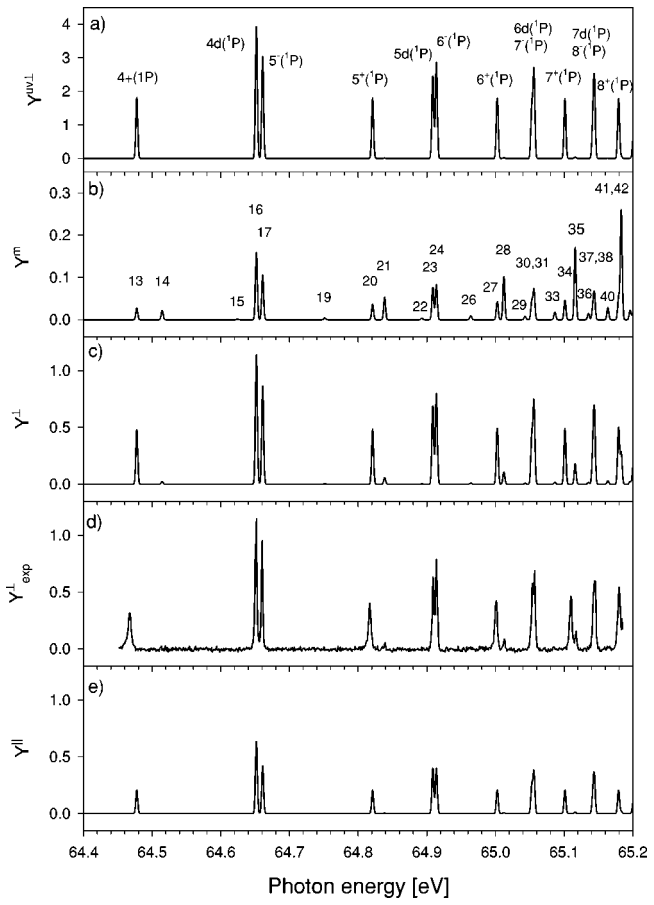

FIG. 5. Calculated yield of uv photons (a) and metastable species (b) hitting the detector surface. The yield of detected particles (c) is to be compared to the measured yield at 90° to the polarization direction of incoming light (d). The yield (e) is expected to be measured at 0° to polarization.

where θ is the angle between the uv photon direction and polarization of the incoming photon beam. The first term is the primary fluorescence contribution and the second term is due to the secondary fluorescence. The total cross section for creation of metastable states is given by

$$\sigma_i^m = \sigma_{i1} + \sigma_{i2}. \tag{23}$$

During the measurements a large area MCP detector was placed opposite the gas needle, which was mounted perpendicular to the photon beam and the polarization axis. Charged particles were rejected by two properly biased grids in front of the detector. In Figs. 5(a) and 5(b) we present the expected yield of uv photons and metastable atoms hitting the detector. Taking $P_2(\cos\theta) \approx -1/2$ over the solid angle subtended by the MCP we have

$$Y_i^{uv\perp} = 4\pi\delta\left[(\sigma_{i0}+\sigma_{i1}+\sigma_{i2})\left(1-\frac{\beta_i}{2}\right)+\sigma_{i0}\left(1-\frac{\beta_{is}}{2}\right)\right],$$

$$Y_i^m = \sigma_i^m. \tag{24}$$

Because of the directionality of the atomic beam it is assumed above that all the metastable atoms hit the detector surface, covering about $\delta = 2\%$ of the whole solid angle [16]. To make a fair comparison to the measured spectrum the calculated yields were blurred by a Gaussian of 3 meV full width at half maximum representing approximately the energy profile of the incoming light; the largest natural linewidth in the range of the experimental spectrum in Fig. 5(d) is expected to be only 0.12 meV, for the $4^+(^1P)$ line. To simulate the experimental spectrum we have to account for different detector efficiencies for metastable atoms and uv photons. By introducing the efficiency ratio, the signal on the MCP detector is expected to be

$$Y_i^{\perp} = \frac{\epsilon_{uv}}{\epsilon_m} Y_i^{uv\perp} + Y_i^m. \tag{25}$$

The primary and secondary uv photon efficiencies are taken to be equal, in accordance with the experimental data, showing one-half of the yield drop just above the $N=2$ threshold [16]. The unknown efficiency ratio in Eq. (25) was selected in such a way as to obtain the best matching of relative line intensities with the experimental spectrum,

$$\frac{\epsilon_{uv}}{\epsilon_m} \approx \frac{1}{4}. \tag{26}$$

No measurements were taken in similar conditions with the MCP axis parallel to the polarization. Making a similar approximation as above we estimate

$$Y_i^{uv\parallel} = 4\pi\delta[(\sigma_{i0}+\sigma_{i1}+\sigma_{i2})(1+\beta_i)+\sigma_{i0}(1+\beta_{is})], \tag{27}$$

and zero for the metastable yield because the gas inlet is now perpendicular to the polarization. The expected yield of detected particles

$$Y_i^{\parallel} = \frac{\epsilon_{uv}}{\epsilon_m} Y_i^{uv\parallel}$$

with the efficiency ratio (26) is presented in Fig. 5(e). At 0° to polarization we expect about one-half of the yield detected at 90°.

VIII. CONCLUSIONS

We have studied the decay of helium doubly excited states with $n \leqslant 8$ and $J=1$ in order to simulate recent experimental data showing peaks at positions of triplet resonances in the metastable atoms plus uv photon channel. The simulation required calculation of correlated doubly excited states below the $N=2$ threshold. To evaluate the relative importance of the two competing decay channels we have studied primary fluorescence, leading to the singlet and triplet $1snd$ and $1snd$ states below the first ionization threshold, and autoionization, which brings the atom into the ionic ground state. We note that the primary fluorescence rate is in general smaller than the $2p \rightarrow 1s$ fluorescence rate of the helium ion, due to correlated motion of the electrons. To estimate the production cross section of four long lived final states, we followed the relaxation via the fluorescence channel for each

resonance. For this purpose we calculated the array of dipole transition rates connecting all pairs in the set of states $1sn(s,p,d,f)$ with $n \leqslant 8$; they are in good agreement with previously tabulated values [25]. The effective asymmetry parameters of the primary uv emission were calculated to be negative for the predominantly singlet and positive for the predominantly triplet resonances. The asymmetry parameter of the secondary uv emission is expected to be slightly negative. Combining all the calculated results, good agreement was found with the experimental data, measured at 90° to the polarization direction of the incoming light, provided we allow for about four times more efficient detection of helium metastable atoms than uv photons on the standard MCP detector. Taking about 10% detection efficiency for uv photons [31], this result indicates that MCP detection efficiency for helium metastable atoms is close to 40%. An independent measurement of the asymmetry parameters and of the efficiency ratio would be necessary in order to fully verify these results.

We have shown that spin-orbit interaction with all its consequences can indeed explain the measured spectrum, which confirms the interpretation given earlier [16]. Also, it seems that the correlated nature of the doubly excited states manifests itself not only in asymmetric autoionization rates of different series but also in asymmetric fluorescence rates although the photon emission always happens relatively close to the nucleus and the outer electron is far away from it most of the time. Lifetime measurements with time resolution below 1 ps would be necessary to experimentally confirm this phenomenon. Finally, our data may be useful in further experiment planning, probably in the direction of measuring the angular resolved coincidence signal of uv photons, metastable atoms, ions, or electrons, which all appear as decay products of these resonances.

[1] R.P. Madden and K. Codling, Phys. Rev. Lett. **10**, 516 (1963).
[2] J.W. Cooper, U. Fano, and F. Prats, Phys. Rev. Lett. **10**, 518 (1963).
[3] M. Domke, G. Remmers, and G. Kaindl, Phys. Rev. Lett. **69**, 1171 (1992).
[4] K. Schulz, G. Kaindl, M. Domke, J.D. Bozek, P.A. Heimann, A.S. Schlachter, and J.M. Rost, Phys. Rev. Lett. **77**, 3086 (1996).
[5] D.R. Herrick and O. Sinanoglu, Phys. Rev. A **11**, 97 (1975).
[6] C.D. Lin, Phys. Rev. A **29**, 1019 (1984).
[7] Jan M. Rost, K. Schultz, M. Domke, and G. Kaindl, J. Phys. B **30**, 4663 (1997).
[8] M.K. Odling-Smee, E. Sokell, P. Hammond, and M.A. MacDonald, Phys. Rev. Lett. **84**, 2598 (2000).
[9] J.E. Rubensson, C. Sathe, S. Cramm, B. Kessler, S. Stranges, R. Richter, M. Alagia, and M. Coreno, Phys. Rev. Lett. **83**, 947 (1999).
[10] P. Lablanquie, F. Penent, R.I. Hall, J.H.D. Eland, P. Bolognesi, D. Cooper, G.C. King, L. Avaldi, R. Camilloni, S. Stranges, M. Coreno, K.C. Prince, A. Muehleisen, and M. Zitnik, Phys. Rev. Lett. **84**, 431 (2000).
[11] R.D. Cowan, *The Theory of Atomic Structure and Spectra* (University of California Press, Berkeley, 1981).
[12] T.W. Gorczyca, J.E. Rubensson, C. Sathe, M. Ström, M. Agaker, D. Ding, S. Stranges, R. Richter, and M. Alagia, Phys. Rev. Lett. **85**, 1202 (2000).
[13] R.P. Madden, D.L. Ederer, and K. Codling, Phys. Rev. **177**, 136 (1969).
[14] S.E. Canton-Rogan, A.A. Wills, T.W. Gorczyca, M. Wiedenhoeft, O. Nayandin, Chen-Nan Liu, and N. Berrah, Phys. Rev. Lett. **85**, 3113 (2000).
[15] K. Codling, R.P. Madden, and D.L. Ederer, Phys. Rev. **155**, 26 (1967).
[16] F. Penent, P. Lablanquie, R.I. Hall, M. Žitnik, K. Bučar, S. Stranges, R. Richter, M. Alagia, P. Hammond, and J.G. Lambourne, Phys. Rev. Lett. **86**, 2758 (2001).
[17] L. Lipsky, R. Anania, and M.J. Conneely, At. Data Nucl. Data Tables **20**, 127 (1977).
[18] C.N. Liu, M.K. Chen, and C.D. Lin, Phys. Rev. A **64**, 010501(R) (2001).
[19] P. Altick and E.N. Moore, Phys. Rev. Lett. **15**, 100 (1965).
[20] C. Froese Fischer, T. Brage, and P. Jönsson, *Computational Atomic Structure* (Institute of Physics, London, 1997).
[21] I. Lindgren and J. Morrison, *Atomic Many-Body Theory*, Springer Series in Chemical Physics Vol. 13 (Springer, Berlin, 1982).
[22] J.-G. Wang, T.-Q. Chang, and Y.-Z. Qu, Eur. Phys. J. D **2**, 231 (1998).
[23] G. Feinberg and J. Sucher, Phys. Rev. Lett. **26**, 681 (1971).
[24] R.S. Van Dyck, C.E. Johnson, and H.A. Shugart, Phys. Rev. A **4**, 1327 (1971).
[25] C.E. Theodosiou, At. Data Nucl. Data Tables **36**, 97 (1987).
[26] R.N. Zare, *Angular Momentum, Understanding Spatial Aspects in Chemistry and Physics* (Wiley, New York, 1988).
[27] H. Klar, J. Phys. B **13**, 2037 (1980).
[28] H.O. Dickinson and M.R.H. Rudge, J. Phys. B **3**, 1284 (1970).
[29] J.G. Lambourne, M.K. Odling-Smee, J. Harries, P. Hammond, S. Stranges, R. Richter, M. Coreno, and M. Ferianis (unpublished).
[30] K. Prince *et al.*, J. Synchrotron Radiat. **5**, 565 (1998).
[31] *Electron Multiplier Handbook for Mass Spectrometry Applications* (Galileo Electro-Optic Corporation, Sturbridge, MA, 1991).